








A spinwave Ising machine

Artem Litvinenko ¹✉, Roman Khymyn ¹, Victor H. González ¹, Roman Ovcharov ¹, Ahmad A. Awad ^{1,2,3}, Vasyl Tyberkevych⁴, Andrei Slavin ⁴ & Johan Åkerman ^{1,2,3}✉

Time-multiplexed Coherent Ising Machines (CIMs) have demonstrated promising results in rapidly solving large-scale combinatorial problems. However, CIMs remain relatively large and power-demanding. Here, we demonstrate a spinwave-based Ising machine (SWIM) that due to the low spinwave group velocity allows for sufficient miniaturization and reduced power consumption. The SWIM is implemented using a 10-mm-long 5- μm -thick Yttrium Iron Garnet film with off-the-shelf microwave components and can support an 8-spin MAX-CUT problem and solve it in less than 4 μs consuming only 7 μJ . As the SWIM minimizes its energy, we observe that the spin states can demonstrate both uniform and domain-propagation-like switching. The developed SWIM has the potential for substantial further miniaturization with reduction of power consumption, scalability in the number of supported spins, increase of operational speed, and may become a versatile platform for commercially feasible high-performance solvers of combinatorial optimization problems.

¹Department of Physics, University of Gothenburg, Fysikgränd 3, Gothenburg 412 96, Sweden. ²Center for Science and Innovation in Spintronics, Tohoku University, 2-1-1 Katahira, Sendai 980-8577, Japan. ³Research Institute of Electrical Communication, Tohoku University, 2-1-1 Katahira, Sendai 980-8577, Japan. ⁴Department of Physics, Oakland University, 146 Library Drive, Rochester, MI 48309, USA. ✉email: artem.litvinenko@physics.gu.se; johan.akerman@physics.gu.se

As Moore's law comes to an end due to physical limitations, and the need for data processing continues to grow, unconventional analog and digital computing paradigms are being investigated. Many modern data processing tasks involve combinatorial optimization problems and require special-purpose accelerators for fast and power-efficient computing. Combinatorial optimization is essential to select the optimal path from an enormous range of choices and appears in various social and industrial fields such as optimizing financial transactions¹, logistics, travel², circuit layout design³, genetic engineering and molecular design for chemical discovery⁴. Conventional computers based on Von Neumann architectures are inefficient in solving hard combinatorial optimization problems due to the factorial growth of all possible combinations if evaluated using brute force. Fortunately, Ising machines have emerged as a promising non-von-Neumann computing scheme that can accelerate the computation of such NP-hard optimization problems.

An Ising machine maps an NP-problem onto the Ising Hamiltonian of an array of N binarized and interacting physical entities, commonly referred to as spins $s_i = \pm 1$.

$$H(s_1, \dots, s_N) = -\sum_{i < j} J_{ij} s_i s_j - \sum_{i=1}^N h_i s_i \quad (1)$$

A specific problem is coded by adjusting the pairwise coupling terms, J_{ij} , such that the lowest energy spin glass configuration represents the solution to the NP-problem. This is possible because spin glass solutions belong to the NP-hard complexity class⁵, and many NP-complete and NP-hard problems can be reformulated as Ising Hamiltonians⁶. Then, the energy minimization of the entire array can be employed as a solution search algorithm in a process called annealing⁷.

Various types of Ising machines⁷ have been proposed in the recent decades exploiting novel physical building blocks such as spintronic devices^{8–10}, memristor crossbars¹¹, quantum superconducting junctions¹², metal-insulator relaxation oscillators¹³, and degenerate optical parametric oscillators^{14,15}, as well as conventional CMOS technology with analog electric oscillators^{16,17}, and field programmable gate arrays (FPGAs)¹⁸. In particular, optical Coherent Ising Machines (CIM)^{14,15} have attracted great attention due to their high computational speed, a time-multiplexing method that provides all-to-all Ising spin connections, and the largest amount of supported Ising spins amongst all implementations. Nevertheless, the commercial feasibility of optical CIMs remains elusive as the technology requires optical tables, kilowatts of power, and kilometers of optical fibers, which altogether blocks its further development from a proof-of-principle demonstration to a miniaturized commercially viable device.

In this work, we present a time-multiplexed spinwave Ising machine (SWIM) with artificial spin states implemented via the phase of spinwave radio-frequency (RF) pulses propagating in an Yttrium Iron Garnet (YIG) thin film. Spinwaves are a fundamental type of collective excitations in magnetic systems^{19,20} and are being actively used for the implementation of signal processing^{21,22}, frequency synthesis^{23,24}, logic^{25,26} and computing^{27–29} applications due to their inherent non-linearities and exceptionally slow propagation velocities that is 5–7 orders of magnitude slower than the speed of light in optical fibers. Another advantage comes from the simplicity and efficiency of microwave current-to-spinwave transducers and the off-the-shelf availability of affordable and power-efficient microwave electronic components, which reduces the power consumption to only milliwatts of power in contrast to optical kilowatt-power parametric phase-sensitive amplifiers. Altogether, the use of propagating spinwaves, for the design of a time-multiplexed Ising machine, defines a path from a laboratory demonstrator to

a commercially feasible technology with potential for CMOS integration.

Results

Theoretical description of spinwaves. The spinwave propagation properties depend on the strength and orientation of the static magnetic field applied to the film and on the magnetic properties of its material, such as its saturation magnetization (M_s), exchange stiffness (A), and gyromagnetic ratio (γ). In this work, the static magnetic field is applied at angle $\theta = 53^\circ$ *w.r.t.* to the film plane, with its in-plane component parallel to the antennas, *i.e.* perpendicular to the spinwave propagation along the waveguide. The excitation frequency is described by the dispersion relation^{19,20}:

$$\omega_0 = \gamma \mu_0 \sqrt{(H_{\text{int}} + M_s l_{\text{ex}}^2 k^2)(H_{\text{int}} + M_s l_{\text{ex}}^2 k^2 + M_s F_0)}, \quad (2)$$

$$F_0 = P_0 + \cos^2 \theta_{\text{int}} [1 - P_0 + M_s P_0 (1 - P_0) / (H_{\text{int}} + M_s l_{\text{ex}}^2 k^2)], \quad (3)$$

where k is the full wavevector of the spinwave, $P_0 = 1 - (1 - \exp(-kd))$ and $d = 5 \mu\text{m}$ being the thickness of the film, $l_{\text{ex}} = \sqrt{2A/(\mu_0 M_s^2)} \simeq 1.7 \cdot 10^{-8}$ m the exchange length for YIG, and H_{int} and θ_{int} define the value and out-of-plane angle of the internal field; these can be found from the strength and angle of the applied field (H and θ) using the solution of the magnetostatic problem¹⁹. In our case $\mu_0 H = 0.04$ T and $\theta = 53^\circ$ were chosen as it was empirically found to yield a high excitation efficiency and low total losses in the YIG delay line when using simple thin copper wire antennas.

Design and performance of the spinwave Ising Machine. The SWIM employs a time-multiplexing approach similar to optical CIMs^{14,15,30–35} but in the microwave frequency domain, which leads to certain signal processing modifications and substantially enhanced performance. As shown in Fig. 1a, it consists of two blocks: (i) an electronic part for linear and parametric amplification of the RF pulses, RF pulse interconnection, and RF pulse measurement, and (ii) a physical YIG spinwave waveguide where all the spinwave RF pulses are excited by a first transducer (antenna), allowed to propagate along the film length, and finally transformed back to microwave RF pulses by a second transducer. In contrast to optical CIMs, where optical pulses propagate and are amplified in an optical ring system, never leaving the ring, the SWIM is a multi-physical system where amplification of the propagating RF pulses and their further signal processing is performed outside of the YIG waveguide in a power-efficient electronic system. This is possible because the carrier frequency of the propagating spinwaves is around 3 GHz and, therefore, can be easily handled by inexpensive and readily available commercial RF components.

Figure 1b shows the spinwave spectrum of the YIG spinwave waveguide in the form of its S_{21} -parameter. The propagation and inter-conversion losses in the YIG delay line sum up to 39 dB of the total attenuation which can be easily compensated by linear and phase-sensitive amplifiers. Moreover, relatively small attenuation of the YIG delay line and high power threshold allow for high signal-to-noise ratio in the system. The SNR of the propagating signals in the main loop is 64 dB. The SNR of the coupling pulses reaches 56 dB, which allows to use coupling coefficients with high resolution. The details of the calculation of the SNR and coupling accuracy can be found in Supplementary Note 3.

A major advantage of using spinwaves is their 5–7 orders of magnitude slower propagation than the speed of light in optical fibers, which allows us to reduce the length of the YIG waveguide

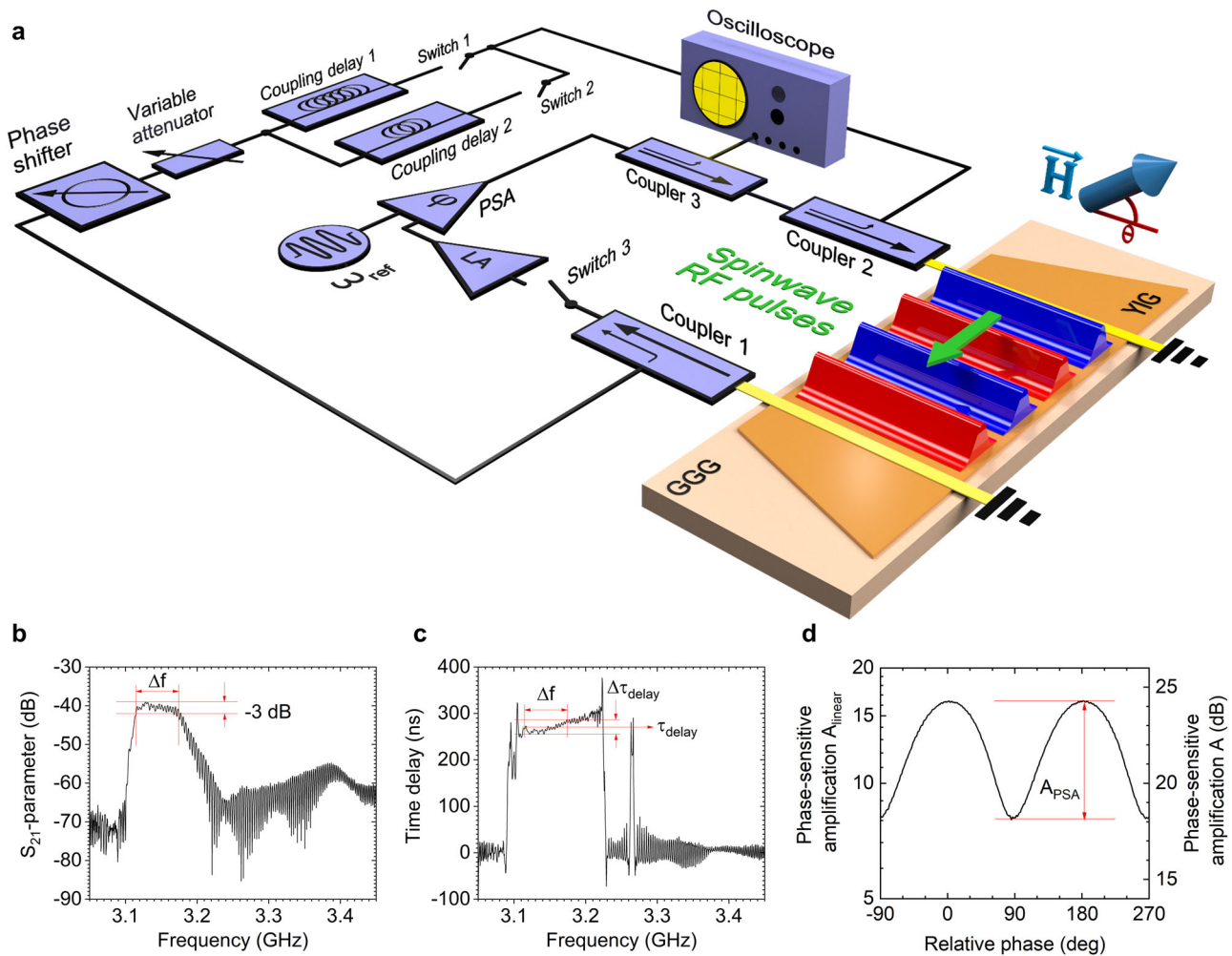


Fig. 1 The spinwave Ising machine (SWIM). **a** Schematic of the SWIM with a Yttrium Iron Garnet (YIG) waveguide on Gadolinium Gallium Garnet (GGG) substrate, peripheral microwave components described in the text, and a real-time oscilloscope for direct studies of the time-evolution of all spins; couplings between spins are implemented using three delay cables of different lengths. **b** Measurement of the S_{21} of the YIG delay line showing the spinwave spectrum. $\Delta f = 60$ MHz is the spinwave spectral bandwidth measured at -3 dB. **c** The frequency-dependent delay time of the YIG delay line. $\tau_{\text{delay}} = 271$ ns is the average delay time over Δf with a total deviation of $\Delta\tau_{\text{delay}} = 30$ ns. **d** Amplification of the parametric phase-sensitive amplifier as a function of the relative phase between the propagating RF pulses and the reference signal $\omega_{\text{ref}} = 6.25$ GHz, with a phase sensitivity of $A_{\text{PSA}} = 6.1$ dB.

to millimeters compared to the kilometers-long optical fibers of CIM. As our artificial Ising spins consist of spinwave RF pulses of length τ_p , the maximum number of supported spins is $N = \tau_{\text{delay}} / \tau_p$, where the waveguide delay time $\tau_{\text{delay}} = l_{\text{YIG}} / v_{g,\text{sw}}$ is the ratio of the waveguide length (l_{YIG}) and the spinwave group velocity ($v_{g,\text{sw}}$). The minimum duration of the spinwave radio-pulse forming the artificial Ising spin in the SWIM is determined by: (i) the value of the 3-dB frequency bandwidth Δf of the spinwave spectrum, which controls the slew rate of the spinwave RF pulses, and (ii) the variation of the spinwave delay time $\Delta\tau_{\text{delay}}$ within the same 3-dB bandwidth Δf , which broadens the pulses as they propagate between the two transducers. The time delay deviation originates from a spinwave dispersion ((2),(3)) and can be efficiently compensated using different techniques such as soliton formation³⁶, combination of different types of spinwaves^{37,38}, the use of multi-layer YIG films³⁹.

The bandwidth of the spinwave generation spectrum (see Fig. 1b) is $\Delta f = 60$ MHz measured at the -3 dB level. Figure 1c shows the corresponding frequency-dependent delay time, with an average value across Δf of $\tau_{\text{delay}} = 271$ ns and a deviation of 30.2 ns. The limit of minimal pulse width derived from Δf is 16.8 ns. However, the delay time deviation causes a significant

broadening of the propagating spinwave RF pulses limiting the total minimal pulse width to 34 ns and, consequently, the SWIM spin capacity to 8 spins.

In contrast to optical CIMs^{14,15,30} where the pulses are formed via a pulsed reference pumping source, here in SWIM we use a constant reference signal and in order to define artificial Ising spins in the form of separate time-multiplexed RF propagating pulses, we introduce an RF switch 2 that is triggered by a square wave signal with variable frequency to control the spinwave RF pulse length, τ_p , and the repetition rate f_{switch} . The use of a constant reference signal and modulated loop demonstrates a better result in terms of signal stability and allows to partially compensate pulse broadening caused by spinwave dispersion and consecutive delay time deviation. The details on the circuit design can be found in Supplementary Note 1.

A phase-sensitive amplifier (PSA) limits conditions for stable oscillations in the SWIM ring circuit to only signals at either phase 0 or π relative to a pumping reference signal at twice the oscillating frequency 3.125 GHz (see Fig. 1d); this consequently phase-binarizes the system. The PSA also induces second-harmonic frequency locking to the external reference signal 6.250 GHz, which further improves the frequency stability. Here,

we implemented a phase-sensitive amplifier with conventional microwave components that have a low nonlinearity threshold and, therefore, consume below 1 W which can potentially be further reduced. We note that works in the literature^{40–42} report on the design of parametric phase-sensitive amplifiers implemented as additional transducers or resonators placed on the YIG delay. Using spinwave parametric amplifiers can potentially improve the miniaturization of the SWIM by integrating the spinwave delay line with a phase-sensitive amplifier, especially if implemented at the nanoscale. However, in practice at the mm-scale such phase-sensitive amplifiers require a high pumping power of around 1 W and demonstrate only an improvement in the attenuation rather than a sufficient amplification. This motivated us to use a conventional electronic PSA. The details on the implementation of the PSA can be found in Supplementary Note 2.

Experiment. In order to evaluate the computational performance of the SWIM we use 4-spin and 8-spin MAX-CUT optimization problems. While we have successfully populated the waveguide with up to 10 spins, in agreement with the theoretical estimate above, we here limit the problem size to eight spins to avoid any undesired interference between neighbor spinwave RF pulses, as they may partially overlap.

The first experiment demonstrates the principle of operation and routes for obtaining a solution to the simple 4-spin MAX-CUT problem with antiferromagnetic nearest-neighbor couplings described by the following Ising matrix:

$$J_{ij} = \begin{pmatrix} 0 & -1 & 0 & 0 \\ 0 & 0 & -1 & 0 \\ 0 & 0 & 0 & -1 \\ -1 & 0 & 0 & 0 \end{pmatrix} \quad (4)$$

This asymmetric matrix can be realized using a single Coupling delay cable 1 with a delay time of 68 ns, i.e. of exactly one period of the pulse repetition time. The asymmetric coupling scheme was chosen for the sake of system simplicity for the demonstration—it only requires a single delay RG-58 cable of 21 m. It would require an additional delay cable of 62 m with 204 ns of delay to implement a symmetric connection scheme. We note that the use of the delay cables was chosen solely for the purpose of our proof-of-concept demonstration. In a large-scale SWIM, an FPGA interconnection block can be used, similar to the CIM implementations^{14,15,30}.

For a 4-spin MAX-CUT problem, Switch 2 is closed and Switch 1 is open to enable delay cable 1 with a delay time of 68 ns, i.e. or exactly one period of the pulse repetition time. Each microwave RF pulse passing through Coupler 2 generates both a spinwave RF pulse in the YIG delay line and a 1:10 ratio coupling microwave RF pulse propagating through the Coupling delay cable 1. After 68 ns, the coupling microwave RF pulse reaches the Coupler 1 (also 1:10) and combines with a different microwave RF pulse converted from a propagating spinwave RF pulse, effectively implementing the coupling between these two spins. Taking into account the coupling coefficients of the couplers, and the propagation losses in the coupling delay cable, the ratio between the amplitude of the propagating RF pulses and the coupling signal is -8 dB and can be further reduced by the variable attenuator. The level of -8 dB in electrical coupling corresponds to $J_{ij}=1$ for MAX-CUT problems with 1-bit resolution of coupling coefficients and can be renormalized if the attenuation is used. The negative sign of the coupling coefficients J_{ij} is realized using an additional 180° degree phase shift implemented with a variable phase shifter.

For a demonstration of the computational dynamics, the SWIM is first placed in a randomly chosen steady state $s_j^1 = \{+1 -1 -1 -1\}$ (Fig. 2a) with the Coupling cables 1 and 2 disconnected by opening the switches 1 and 2. The value $+1$ corresponds to 180° of phase difference between the RF pulse and the reference signal ω_{ref} , while the value -1 corresponds to 0° phase difference. The time traces of control signals V_{switch} , the signals of propagating RF pulses V_{ampl} and their instantaneous phase are shown in Fig. 2d–l, where the color of the time traces (Fig. 2g–i) corresponds to their instantaneous phases. As can be seen, the propagating spinwave RF pulses are well-defined and separated from each other; their individual phases are similarly well-defined and uniform in time. The initial s_j^1 represents a non-optimal MAX-CUT solution with the number of cuts equal to 2 (see Fig. 2a). At $t=0$, we connect the Coupling delay cable 1 by closing the switch 1 and let the SWIM evolve for $3.8 \mu\text{s}$ or 14 circulation periods, during which it reaches a stable state and finds the optimal number of cuts. Figure 2b, h, k shows the resulting spin state during the 14th circulation period, where the third spin has now switched its phase to π under the influence of the coupling matrix. The SWIM has hence changed its state to $s_j^{12} = \{+1 -1 +1 -1\}$, which represents an optimal solution with the number of cuts equal to 4 (see Fig. 2b). A simple theoretical model, which describes this case can be found in Supplementary Note 5.

Similarly, we confirmed the SWIM's capability to solve an 8-spin MAX-CUT problem with nearest-neighbor asymmetrical coupling scheme (see Fig. 2c, f, i, l). The frequency f_{switch} of RF Switch 3 was hence increased to 29.6 MHz to increase the spin capacity to eight. As the corresponding repetition period decreased to 34 ns, a shorter Coupling delay cable 2 with 34 ns delay was used for this experiment. As can be seen in Fig. 2i the spinwave RF pulses start to show some minor overlap, which could nevertheless be neglected, as the SWIM still reached the correct solution when interrogated after 14 cycles.

In order to visualize the routes to a solution and the evolving dynamics of the circulating RF pulses, signal envelopes and the instantaneous phases for the 3rd spin for both 4- and 8-spin MAX-CUT problems were captured at fourteen consecutive circulation steps and compiled into Fig. 3a–c in the form of overlapping traces with different colors corresponding to the number of circulations. We observed that the SWIM demonstrates two different switching modes. The first scenario is observed for the 4-spin MAX-CUT problem (see Fig. 3a, c) where the RF pulses are longer (40 ns). During the first 6 circulations, the spinwave RF pulse gradually separates into two distinct domains of approximately equal size separated by a domain wall that can be clearly seen in the instantaneous phase. From this point on, the domain wall starts to propagate through the pulse until a fully switched single domain pulse is established at about the 10th cycle. A different switching mechanism can be observed for the 8-spin MAX-CUT problem (see Fig. 3b, d) with the 34 ns long Coupling delay cable 2. In this case, the evolution of the instantaneous phase occurs via a gradual and uniform shift from around 0 to π . It is possible that the shorter pulse length in the 8-spin case promotes a more uniform response to the coupling. The details on the evolution of spins can be found in Supplementary Note 4. Regardless of its origin, this gradual uniform switching mechanism might open up the possibility to use the SWIM concept as a potential platform to implement XY machines⁴³.

A key parameter for benchmarking the performance of an Ising machine is its time-to-solution. In order to estimate averaged time-to-solution parameter, we perform an experiment where we periodically switch off the amplification in the loop for $2 \mu\text{s}$ by

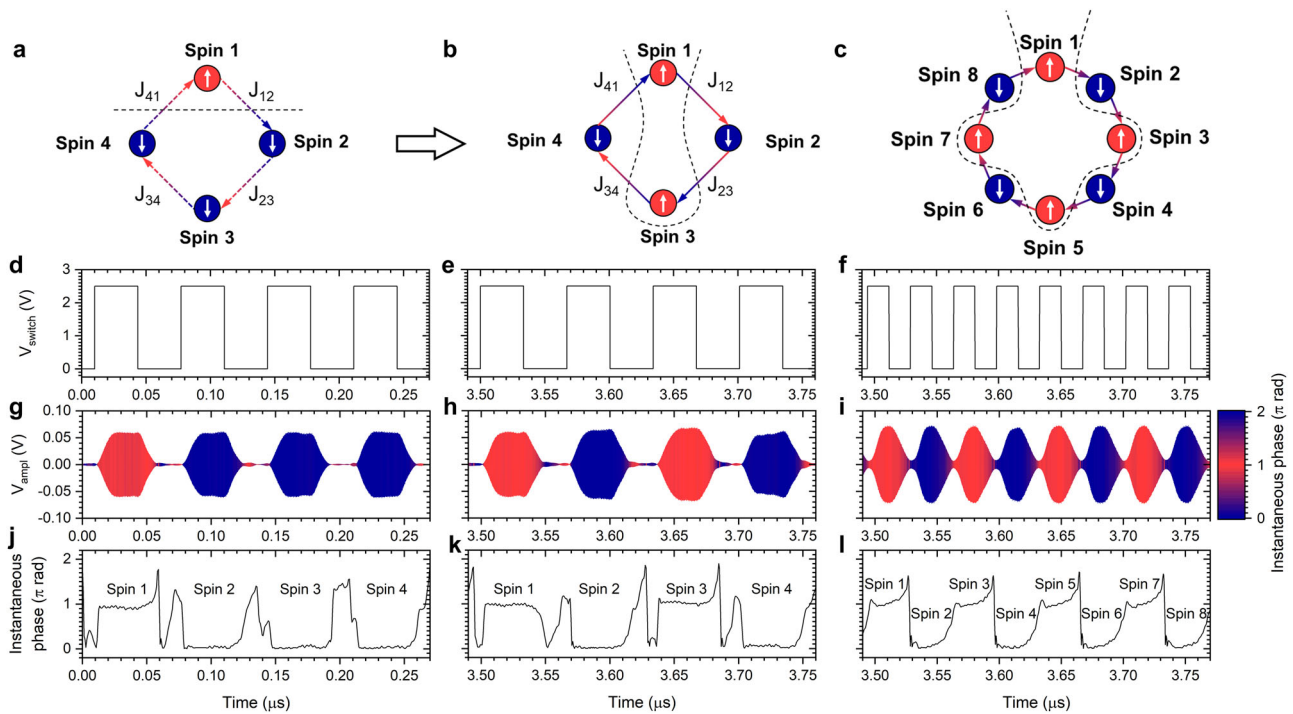


Fig. 2 Experimental demonstration of 4-spin SWIM solving a MAX-CUT problem. **a, b** Transformation of the initial non-optimal state (**a**) to an optimal solution (**b**) for 4-spin MAX-CUT optimization problem. The number of cuts for the MAX-CUT problem is determined by the total number of couplings that cross the line separating the spins into two groups, considering their regrouping based on their spin values. **c** An optimal solution for 8-spin MAX-CUT optimization problem with eight cuts. SWIM control traces for 4-spin (**d, e**) and 8-spin (**f**) problems. Amplified signals of RF propagating pulses in the initial non-optimal state (**g**) of MAX-CUT 4-spin and the final solutions of MAX-CUT 4-spin problem (**h**) and 8-spin problem (**i**). A control signal of switch 3 has a repetition frequency of $f_{\text{switch}} = 14.8$ MHz (**d, e**) for 4-spin problem and 29.6 MHz (**f**) for 8-spin problem and duty cycle of 50% that forms oscillations in the SWIM ring oscillator into separate propagating RF pulses. Calculated instantaneous phase signals for 4-spin problem (**j, k**) and 8-spin problem (**l**). The time traces in (**g-i**) are colored according to a value of the calculated instantaneous signal to visually show the pulse instantaneous phase. Since the time intervals shown are much longer than the oscillation period of the propagating pulses V_{amp} ($1/3.125$ GHz = 0.320 ns), individual oscillations are not resolved and merge into a colored continuum.

controlling supply voltage of the linear amplifier V_{ctrlamp} (see Fig. 4a) to ensure that the SWIM returns to an idle state, after which we again switch on the loop amplification. Figure 4b, c shows the temporal evolution of the SWIM prior to and after shutdown. It first takes $1.9 \mu\text{s}$ for the SWIM to develop circulating RF pulses to saturation level. It then takes an additional $1.5 \mu\text{s}$ to reach a stable state that represents the optimal solution. The rapid development of the amplitude of the circulating pulses is explained by a relatively high overcompensation of signal losses in the loop of the ring-based SWIM circuit (~ 2 dB).

The SWIM design allows for the control of the overall coupling strength between spins by attenuating the signal coming from the coupling delay cables with a variable attenuator (see Fig. 1a). To benchmark the SWIM dynamic range, a series of ten consecutive time-to-solution measurements were conducted at different coupling attenuation for the 4-spin MAX-CUT problem. A statistical analysis is presented in Fig. 4d. For this very simple problem, the SWIM demonstrates almost constant time-to-solution values for attenuation levels from 0 to 12 dB with about 20 circulations or $5 \mu\text{s}$. The very weak trend of a longer time-to-solution at higher coupling attenuation is then more pronounced at 15 dB. The large SWIM dynamical range of 15 dB should allow the mapping of optimization problems with high range and resolution of coupling coefficients in the Ising matrix.

Operational principles. In order to achieve optimal solutions in the simple cases of 4- and 8-spin MAX-CUT problems where there are no local minima, a single dynamical run appears

sufficient. However, in large hard optimization problems with dense coupling graphs, there may exist a number of local minima in the Ising Hamiltonian. The search for an optimal or exact solution in such cases can be implemented with a classical annealing scheme⁴⁴ by inducing thermal fluctuations in the state of the spins after stabilization of the system in local minima. In SWIM it can be implemented by injecting additional signal to the loop with random phase state that would force chosen RF pulses to change their state. The SWIM has the same architecture as CIMs and can operate under the minimum gain principle³¹. The amplification in the loop can be gradually increased with voltage-controlled analog or digital attenuators giving enough time for the system to start up at the lowest energy state that corresponds to the minimum state of the Ising Hamiltonian.

Discussion

The presented SWIM was implemented with μm -thick YIG waveguides having mm-scale lateral dimension. However, in the recent decade, magnonics has made significant progress in scalability demonstrating nanometer-thick YIG-based waveguides^{45,46} and signal processing devices^{25,47} with sub-micrometer channel width. At the nanoscale, the spinwave bandwidth exceeds hundreds of MHz and the delay deviation can be improved with the same methods applicable to mm-scale YIG films. The group velocity of spinwaves in the magnetostatic range is inversely proportional to the thickness of the waveguides and can reach tens of meters per second. This makes it beneficial to exploit nm-thick YIG films with reduced SW

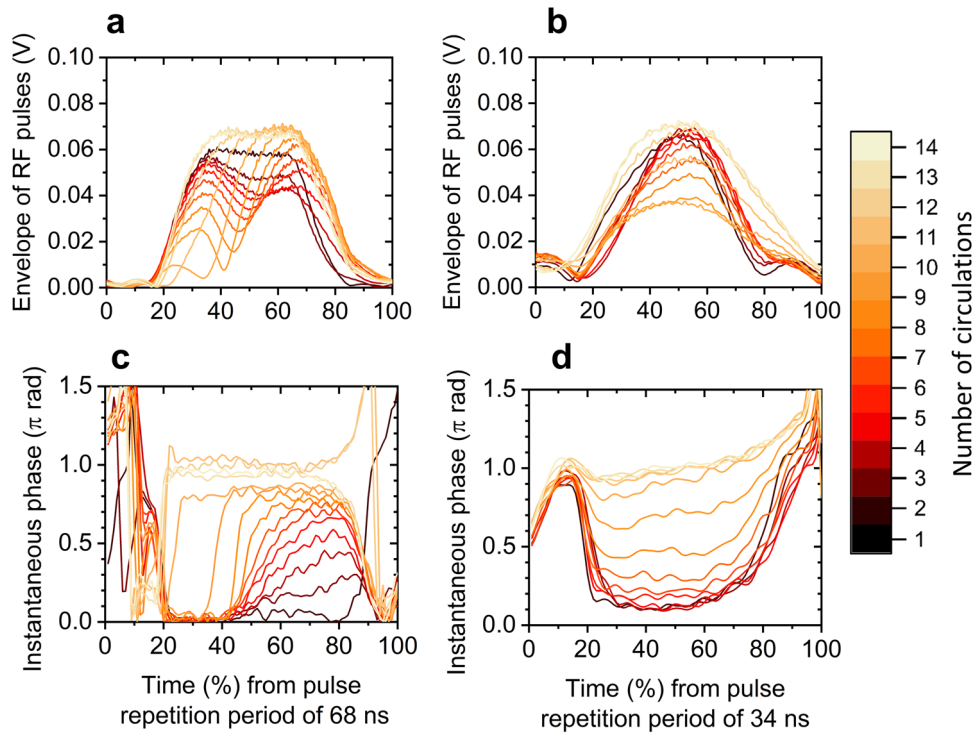


Fig. 3 Spin switching scenarios for 4- and 8-spin MAX-CUT problem computations. Envelopes (a, b) and instantaneous phase signals (c, d) of the 3rd propagating RF pulse signal within 14 circulation periods plotted in the form of overlapping traces in a relative scale for 4-spin (a, c) and 8-spin (b, d) MAX-CUT optimization problem. The color of the time traces corresponds to the circulation number.

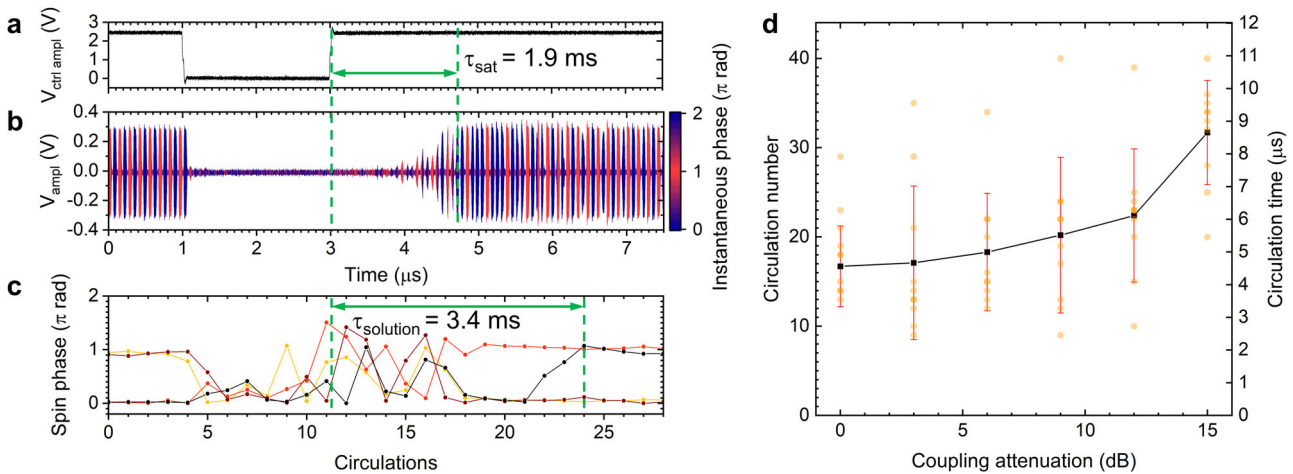


Fig. 4 Measurement of the time-to-solution parameter for 4-spin MAX-CUT problem computation. SWIM time traces for the measurement of time-to-saturation τ_{sat} and time-to-solution $\tau_{solution}$ parameters. **a** A control signal $V_{ctrlampl}$ for the linear amplifier. The linear amplifier switches down at the moment $1 \mu s$ with a blackout period of $2 \mu s$ to ensure signal suppression. **b** An amplified signal of RF propagating pulses V_{ampl} . The time traces in (b) are colored according to a value of the calculated instantaneous signal to visually show the pulse instantaneous phase. **c** Phase values in the center of each propagating RF pulse sampled at each circulation period. Lines and circles are colored according to the number of the circulating RF pulse: Spin 1 - black, Spin 2 - brown, Spin 3 - red, Spin 4 - orange. **d** Mean circulation number and its standard deviation in the form of error bars with corresponding time-to-solution circulation time value for 4-spin MAX-CUT problem as a function of the additional coupling attenuation. Statistics is based on 10 consecutive measurements for each coupling attenuation. Individual points are shown as semitransparent orange circles. Note that some points may overlap.

velocity v_{gr} to downscale the YIG delay line in terms of physical size. Since $v_{gr} = 2\pi\partial f/\partial k$, we suggest using a narrow frequency bandwidth of 200 MHz to operate at a relatively constant group velocity and to reduce the required range of the wavevectors, which, in turn, reduces the requirements for miniaturization of the emitting antennas. With modern advances in magnonics, one can expect a spatial spin length of $\approx 1 \mu m/spin$. With the

required frequency bandwidth of 200 MHz, it limits the minimum SW velocity to 200 m/s.

On the other hand, spinwaves propagating in the YIG film are subject to propagating losses with a lifetime estimated as:

$$\tau_{life}^{-1} = \left(2\pi f \alpha + \frac{\gamma \mu_0 \Delta H_0}{2} \right), \quad (5)$$

where the first term describes Gilbert damping and the second describes inhomogeneous broadening. Recent advances in YIG film growth allow for very low values for both contributions and, as an example, we will use parameters obtained experimentally in⁴⁸ for a 20-nm-thick film. For wavevectors around $k \approx 10^7$ rad/m and frequency $f = 2$ GHz, the group velocity is $v = 600$ m/s and decay time $\tau_{\text{life}} = 550$ ns. Taking into account that modern integrated microwave amplifiers can easily compensate for tens of decibels of signal loss, we suggest a delay line that would have 60 dB of attenuation and a corresponding delay time $\tau_{\text{delay}} = 60\tau_{\text{life}}/8.686 = 3.797 \mu\text{s}$. Thus, using Eq. (5) with the above parameters yields a delay line with a length of just 2.278 mm and 759 spins capacity.

In order to further improve the spin capacity of the proposed SWIM, an array of microscale YIG waveguides can be used to form multiple tracks, each with its own linear and phase-sensitive amplifiers. In a multi-track system, the interconnection between propagating spins can be implemented similarly to CIM with digital FPGA or application-specific integrated circuit (ASIC) blocks. In the case of using N parallel tracks instead of connecting all the delay lines and amplifiers in series in the time-multiplexed architecture of SWIM, the time-to-solution parameter will be improved and reduced by N since the circulation time will be N times shorter and the propagating RF pulses will interact with each other more frequently.

We hence suggest an array of 150 parallel waveguides with a lateral size of $2660 \times 1.0 \mu\text{m}$ each supporting 759 spins. A separation of $10 \mu\text{m}$ between waveguide centers would make cross-talk negligible. Then, with the total lateral size of 2.66×1.5 mm, a multi-track SWIM would have 113,850 spins, i.e. about the same capacity of the most recent CIM¹⁴ with a 5-km thermally-stabilized optical fiber delay system.

Finally, it has been recently demonstrated that propagation losses of spinwaves in nanoscale waveguides can be effectively compensated using different techniques of parametric pumping^{25,49} reducing the constraints for the length of nanoscale YIG waveguides and improving the SWIM potential for scalability in terms of number of spins. The excitation antennas can be replaced with more scalable and energetically efficient multiferroic magnetoelectric cells^{50,51}.

Conclusion

Our work creates a pathway for miniature low-power and commercially feasible Ising machines for solving a wide range of optimization problems. The SWIM concept has a high potential for further scaling in terms of spin capacity and physical size and the improvement of power consumption and speed performance parameters. The exploitation of non-linear spinwave solitons^{52,53} and the proper choice of magnetization angle could compensate spinwave dispersion and flatten delay time over a wide range of frequencies allowing to use shorter spinwave RF pulses effectively increasing the number of supported Ising spins with the same length of YIG waveguide. The use of spinwaves in nm-scale thin YIG films with an exceptionally slow propagation velocity of 0.3–0.6 km/s^{20,54} could provide a way to further miniaturize the YIG waveguide and SWIM size while reaching hundreds of thousands of artificial spins within mm-long spinwave waveguides. Miniaturization opens the possibility of SWIM scaling by parallelizing the system using multiple ring circuits which would improve the time-to-solution parameter by the number of the parallel rings as it decreases the circulation time. Moreover, SWIM has the potential to be implemented similarly to the first realization of CIM³⁵ using integrated spinwave amplifiers^{25,49,55,56} and magnonic logic and, therefore, a future SWIM could potentially also operate in a quantum regime under the minimum gain principle with linear coupling in the analog domain³¹.

Methods

Sample. The lateral dimension of the YIG waveguide is $10 \times 7 \text{ mm}^2$. The microwave-to-spinwave transducers are $50\text{-}\mu\text{m}$ -thin copper wires. The YIG sample is placed on a FR-4 metallized printed circuit board with the Gadolinium Gallium Garnet substrate facing down and copper wire transducers positioned on top of the YIG film.

Electrical measurements. The instantaneous phase dynamics was extracted from V_{ampl} signal time traces using Hilbert transform technique similar to the studies^{57–59}. In order to improve the signal-to-noise ratio and ensure unambiguous phase detection with Hilbert transform technique, the time trace V_{ampl} was initially filtered with a bandpass filter with a central frequency of 3.15 GHz, the bandwidth of 100 MHz and out-of-band suppression of 60 dB.

The group delay presented in Fig. 1c was obtained from phase-delay measurement of the S-parameters using a vector network analyzer. The S-parameters were measured across a wide range of frequencies starting from 3 to 3.5 GHz. The group delay is calculated as the negative derivative of the phase shift with respect to the frequency. This calculation was performed using a built-in function of a vector network analyzer Rohde & Schwarz ZNB 40.

The phase-sensitive amplification curve was extracted from the envelope of an amplified signal with constant amplitude and frequency detuned from the reference signal frequency by 10 MHz. The frequency detuning introduced a continuous phase drift with a period of 100 ns, which allowed a smooth phase-sensitive amplification curve to be extracted. The details on the design of the phase-sensitive amplifier can be found in Supplementary Note 2.

Data availability

The data is available upon reasonable request from corresponding authors.

Received: 20 February 2023; Accepted: 11 August 2023;

Published online: 25 August 2023

References

- Ibarra, O. & Kim, C. Fast approximation algorithms for the knapsack and sum of subset problems. *J. Assoc. Comput. Mach.* **22**, 463–468 (1975).
- Černý, V. Thermodynamical approach to the traveling salesman problem: An efficient simulation algorithm. *J. Optim. Theory Appl.* **45**, 41–51 (1985).
- Barahona, F., Grötschel, M., Jünger, M. & Reinelt, G. An application of combinatorial optimization to statistical physics and circuit layout design. *Oper. Res.* **36**, 493–513 (1988).
- Earl, D. J. & Deem, M. W. Parallel tempering: theory, applications, and new perspectives. *Phys. Chem. Chem. Phys.* **7**, 3910–3916 (2005).
- Barahona, F. On the computational complexity of Ising spin glass models. *J. Phys. A: Math. Gen.* **15**, 3241–3253 (1982).
- Lucas, A. Ising formulations of many np problems. *Front. Phys.* **2**, 5 (2014).
- Mohseni, N., McMahon, P. L. & Byrnes, T. Ising machines as hardware solvers of combinatorial optimization problems. *Nat. Rev. Phys.* **4**, 363–379 (2022).
- Albertsson, D. I. et al. Ultrafast Ising machines using spin torque nano-oscillators. *Appl. Phys. Lett.* **118**, 112404 (2021).
- Houshang, A. et al. Phase-binarized spin Hall nano-oscillator arrays: towards spin Hall Ising machines. *Phys. Rev. Appl.* **17**, 014003 (2022).
- Sutton, B., Camsari, K. Y., Behin-Aein, B. & Datta, S. Intrinsic optimization using stochastic nanomagnets. *Sci. Rep.* **7**, 44370 (2017).
- Cai, F. et al. Power-efficient combinatorial optimization using intrinsic noise in memristor hopfield neural networks. *Nat. Electron.* **3**, 409–418 (2020).
- Johnson, M. W. et al. Quantum annealing with manufactured spins. *Nature* **473**, 194–198 (2011).
- Dutta, S. et al. Experimental demonstration of phase transition nano-oscillator based Ising machine. In *Proc. 2019 IEEE International Electron Devices Meeting*. (IEEE, San Francisco, CA, USA), 37.8.1–37.8.4 (2019).

14. Honjo, T. et al. 100,000-spin coherent Ising machine. *Sci. Adv.* **7**, eabh0952 (2021).
15. Inagaki, T. et al. A coherent Ising machine for 2000-node optimization problems. *Science* **354**, 603–606 (2016).
16. Wang, T., Wu, L. & Roychowdhury, J. New computational results and hardware prototypes for oscillator-based Ising machines. In *Proc. 56th Annual Design Automation Conference 2019* (ACM, New York, NY, USA), 1–2 (2019).
17. Moy, W. et al. A 1,968-node coupled ring oscillator circuit for combinatorial optimization problem solving. *Nat. Electron.* **5**, 310–317 (2022).
18. Tatsumura, K., Yamasaki, M. & Goto, H. Scaling out Ising machines using a multi-chip architecture for simulated bifurcation. *Nat. Electron.* **4**, 208–217 (2021).
19. Kalinikos, B. & Slavin, A. Theory of dipole-exchange spin wave spectrum for ferromagnetic films with mixed exchange boundary conditions. *J. Phys. C: Solid State Phys.* **19**, 7013 (1986).
20. Chumak, A., Serga, A. & Hillebrands, B. Magnonic crystals for data processing. *J. Phys. D: Appl. Phys.* **50**, 244001 (2017).
21. Papp, Á., Porod, W., Csurgay, Á. I. & Csaba, G. Nanoscale spectrum analyzer based on spin-wave interference. *Sci. Rep.* **7**, 1–9 (2017).
22. Ustinov, A. B. & Kalinikos, B. A. A microwave nonlinear phase shifter. *Appl. Phys. Lett.* **93**, 102504 (2008).
23. Litvinenko, A., Grishin, S., Sharaevskii, Y. P., Tikhonov, V. & Nikitov, S. A chaotic magnetoacoustic oscillator with delay and bistability. *Tech. Phys. Lett.* **44**, 263–266 (2018).
24. Litvinenko, A. et al. Tunable magnetoacoustic oscillator with low phase noise. *Phys. Rev. Appl.* **15**, 034057 (2021).
25. Wang, Q. et al. A magnonic directional coupler for integrated magnonic half-adders. *Nat. Electron.* **3**, 765–774 (2020).
26. Khitun, A., Bao, M. & Wang, K. L. Magnonic logic circuits. *J. Phys. D: Appl. Phys.* **43**, 264005 (2010).
27. Watt, S., Kostylev, M., Ustinov, A. B. & Kalinikos, B. A. Implementing a magnonic reservoir computer model based on time-delay multiplexing. *Phys. Rev. Appl.* **15**, 064060 (2021).
28. Marković, D. et al. Easy-plane spin Hall nano-oscillators as spiking neurons for neuromorphic computing. *Phys. Rev. B* **105**, 014411 (2022).
29. Mahmoud, A. et al. Introduction to spin wave computing. *J. Appl. Phys.* **128**, 161101 (2020).
30. McMahan, P. L. et al. A fully programmable 100-spin coherent Ising machine with all-to-all connections. *Science* **354**, 614–617 (2016).
31. Yamamoto, Y. et al. Coherent Ising machines-optical neural networks operating at the quantum limit. *npj Quantum Inf.* **3**, 1–15 (2017).
32. Kako, S. et al. Coherent Ising machines with error correction feedback. *Adv. Quantum Technol.* **3**, 2000045 (2020).
33. Takata, K. et al. A 16-bit coherent Ising machine for one-dimensional ring and cubic graph problems. *Sci. Rep.* **6**, 1–7 (2016).
34. Haribara, Y., Utsunomiya, S. & Yamamoto, Y. *A Coherent Ising Machine for MAX-CUT Problems: Performance Evaluation against Semidefinite Programming and Simulated Annealing*, 251–262 (Springer Japan, Tokyo, Japan, 2016).
35. Marandi, A., Wang, Z., Takata, K., Byer, R. L. & Yamamoto, Y. Network of time-multiplexed optical parametric oscillators as a coherent Ising machine. *Nat. Photonics* **8**, 937–942 (2014).
36. Kalinikos, B., Kovshikov, N. & Slavin, A. Envelope solitons of highly dispersive and low dispersive spin waves in magnetic films. *J. Appl. Phys.* **69**, 5712–5717 (1991).
37. Fetisov, Y. K., Kabos, P. & Patton, C. E. Active magnetostatic wave delay line. *IEEE Trans. Magn.* **34**, 259–271 (1998).
38. Sethares, J., Owens, J. & Smith, C. Msw nondispersive, electronically tunable time delay elements. *Electron. Lett.* **16**, 825–826 (1980).
39. Parekh, J., Chang, K. & Tuan, H. Propagation characteristics of magnetostatic waves. *Circuits, Syst. Signal Process.* **4**, 9–39 (1985).
40. Kolodin, P. A. et al. Amplification of microwave magnetic envelope solitons in thin yttrium iron garnet films by parallel pumping. *Phys. Rev. Lett.* **80**, 1976–1979 (1998).
41. Kostylev, M. & Kalinikos, B. On amplification of the spin wave envelope solitons in ferromagnetic films. *Tech. Phys.* **45**, 277–280 (2000).
42. Bagada, A., Melkov, G., Serga, A. & Slavin, A. Parametric interaction of dipolar spin wave solitons with localized electromagnetic pumping. *Phys. Rev. Lett.* **79**, 2137 (1997).
43. Kalinin, K. P., Amo, A., Bloch, J. & Berloff, N. G. Polaritonic xy-Ising machine. *Nanophotonics* **9**, 4127–4138 (2020).
44. Kirkpatrick, S., Gelatt Jr, C. D. & Vecchi, M. P. Optimization by simulated annealing. *Science* **220**, 671–680 (1983).
45. Jungfleisch, M. B. et al. Spin waves in micro-structured yttrium iron garnet nanometer-thick films. *J. Appl. Phys.* **117**, 17D128 (2015).
46. Collet, M. et al. Spin-wave propagation in ultra-thin yig based waveguides. *Appl. Phys. Lett.* **110**, 092408 (2017).
47. Wang, Q., Chumak, A. V. & Pirro, P. Inverse-design magnonic devices. *Nat. Commun.* **12**, 2636 (2021).
48. Yu, H. et al. Magnetic thin-film insulator with ultra-low spin wave damping for coherent nanomagnonics. *Sci. Rep.* **4**, 1–5 (2014).
49. Verba, R., Carpentieri, M., Finocchio, G., Tiberkevich, V. & Slavin, A. Amplification and stabilization of large-amplitude propagating spin waves by parametric pumping. *Appl. Phys. Lett.* **112**, 042402 (2018).
50. Cherepov, S. et al. Electric-field-induced spin wave generation using multiferroic magnetoelectric cells. *Appl. Phys. Lett.* **104**, 082403 (2014).
51. Verba, R., Carpentieri, M., Finocchio, G., Tiberkevich, V. & Slavin, A. Excitation of propagating spin waves in ferromagnetic nanowires by microwave voltage-controlled magnetic anisotropy. *Sci. Rep.* **6**, 1–9 (2016).
52. Ustinov, A. B., Kalinikos, B. A., Demidov, V. E. & Demokritov, S. O. Generation of dense spin-wave soliton trains in active ring resonators. *Phys. Rev. B* **80**, 052405 (2009).
53. Slavin, A. N., Kalinikos, B. A. & Kovshikov, N. G. *Spin Wave Envelope Solitons in Magnetic Films*. (World Scientific, 9128, Singapore) 209–248 (1994).
54. Merbouche, H. et al. Giant nonlinear self-phase modulation of large-amplitude spin waves in microscopic yig waveguides. *Sci. Rep.* **12**, 1–9 (2022).
55. Padrón-Hernández, E., Azevedo, A. & Rezende, S. Amplification of spin waves by thermal spin-transfer torque. *Phys. Rev. Lett.* **107**, 197203 (2011).
56. Padrón-Hernández, E., Azevedo, A. & Rezende, S. Amplification of spin waves in yttrium iron garnet films through the spin Hall effect. *Appl. Phys. Lett.* **99**, 192511 (2011).
57. Bianchini, L. et al. Direct experimental measurement of phase-amplitude coupling in spin torque oscillators. *Appl. Phys. Lett.* **97**, 032502 (2010).
58. Litvinenko, A. et al. Analog and digital phase modulation and signal transmission with spin-torque nano-oscillators. *Phys. Rev. Appl.* **16**, 024048 (2021).
59. Boashash, B. Estimating and interpreting the instantaneous frequency of a signal. I. fundamentals. *Proc. IEEE* **80**, 520–538 (1992).

Acknowledgements

This work was supported by the Horizon 2020 research and innovation programme, ERC Advanced Grant No. 835068 “TOPSPIN” and the ERC Proof of Concept Grant No. 101069424 “SPINTOP” and the Marie Skłodowska-Curie grant agreement No. 101111429 “SWIM”.

Author contributions

A.L. conceived the concept and designed the circuit; A.L., V.G. and A.A. performed the measurements and analyzed the data; R.K., R.O., A.L. performed theoretical calculations with help from A.S. and V.T.; J.Å. managed the project; all co-authors contributed to the manuscript, the discussion, and analysis of the results.

Funding

Open access funding provided by University of Gothenburg.

Competing interests

A.L., R.K. and J.Å. are inventors of a Swedish patent application (FIK-0145E/2250979-8) that covers the implementation of a spinwave Ising machine using propagating spinwave RF pulses. A.L., R.K. and J.Å. are also co-founders of a spin-off company that aims to develop spinwave-based Ising Machines. All other authors declare no competing interests.

Additional information

Supplementary information The online version contains supplementary material available at <https://doi.org/10.1038/s42005-023-01348-0>.

Correspondence and requests for materials should be addressed to Artem Litvinenko or Johan. Åkerman.

Peer review information *Communications Physics* thanks Gyorgy Csaba and the other, anonymous, reviewers for their contribution to the peer review of this work. A peer review file is available.

Reprints and permission information is available at <http://www.nature.com/reprints>

Publisher's note Springer Nature remains neutral with regard to jurisdictional claims in published maps and institutional affiliations.



Open Access This article is licensed under a Creative Commons Attribution 4.0 International License, which permits use, sharing, adaptation, distribution and reproduction in any medium or format, as long as you give appropriate credit to the original author(s) and the source, provide a link to the Creative Commons licence, and indicate if changes were made. The images or other third party material in this article are included in the article's Creative Commons licence, unless indicated otherwise in a credit line to the material. If material is not included in the article's Creative Commons licence and your intended use is not permitted by statutory regulation or exceeds the permitted use, you will need to obtain permission directly from the copyright holder. To view a copy of this licence, visit <http://creativecommons.org/licenses/by/4.0/>.

© The Author(s) 2023